Longitudinal Study of Optic Disk Perfusion and Retinal Structure in Leber's Hereditary Optic Neuropathy

Giacomo Calzetti,[1–3] Chiara La Morgia,[4] Marco Cattaneo,[1,5] Arturo Carta,[3] Francesca Bosello,[6] Giulia Amore,[7] Michele Carbonelli,[7] Maria Lucia Cascavilla,[8] Stefano Gandolfi,[3] Valerio Carelli,[4,7] Leopold Schmetterer,[1,9–11] Hendrik P. N. Scholl,[1,2] and Piero Barboni[8,12]

[1]Institute of Molecular and Clinical Ophthalmology Basel, Basel, Switzerland
[2]Department of Ophthalmology, University of Basel, Basel, Switzerland
[3]Department of Ophthalmology, University Hospital of Parma, Parma, Italy
[4]IRCCS, Istituto delle Scienze Neurologiche di Bologna, Ospedale Bellaria, Bologna, Italy
[5]Department of Clinical Research, University of Basel, Basel, Switzerland
[6]Department of Neurosciences, Biomedicine and Movement Sciences, Eye Clinic, Ocular Immunology and Neuroophthalmology Service, AOUI-University of Verona, Verona, Italy
[7]Department of Biomedical and Neuromotor Sciences (DIBINEM), University of Bologna, Bologna, Italy
[8]Department of Ophthalmology, University Vita-Salute, IRCCS Ospedale San Raffaele, Milan, Italy
[9]Singapore Eye Research Institute, Singapore National Eye Centre, Singapore
[10]Department of Clinical Pharmacology, Medical University of Vienna, Vienna, Austria
[11]Center for Medical Physics and Biomedical Engineering, Medical University of Vienna, Vienna, Austria
[12]Studio Oculistico d'Azeglio, Bologna, Italy

Corresponding author: Giacomo Calzetti, Institute of Molecular and Clinical Ophthalmology Basel, Mittlere Str. 91, 4056 Basel, Switzerland;
giacomo.calzetti@iob.ch.

PURPOSE. The purpose of this study was to evaluate optic disk perfusion and neural retinal structure in patients with subacute Leber's hereditary optic neuropathy (LHON) and LHON carriers, as compared with healthy controls.

METHODS. This study included 8 patients with LHON in the subacute stage, 10 asymptomatic carriers of a LHON-associated mitochondrial DNA mutation, and 40 controls. All subjects underwent measurement of the retinal nerve fiber layer (RNFL) thickness, the ganglion cell-inner plexiform layer (GCIPL) thickness using optical coherence tomography and optic disk microvascular perfusion (Mean Tissue [MT]) using laser speckle flowgraphy (LSFG). Patients were re-examined after a median interval of 3 months from the baseline visit.

RESULTS. LHON carriers had higher values of RNFL thickness, GCIPL thickness, and disk area than controls ($P < 0.05$), whereas MT was not different between the two groups ($P = 0.936$). Median MT and RNFL thickness were 32% and 15% higher in the early subacute stage of the disease than in controls ($P < 0.001$ and $P = 0.001$). MT declined below the values of controls during the late subacute stage ($P = 0.024$), whereas RNFL thickness declined later during the dynamic stage ($P < 0.001$). GCIPL thickness was lower in patients with LHON than in controls independently of the stage of the disease ($P < 0.001$).

CONCLUSIONS. The high blood flow at the optic disk during the early subacute stage may be the consequence of vasodilation due to nitric oxide release as compensation to mitochondrial impairment. Optic disk perfusion as measured by LSFG is a promising biomarker for LHON diagnosis and monitoring as well as an objective outcome measure for assessing response to therapies.

Keywords: laser speckle flowgraphy, Leber's hereditary optic neuropathy, ocular blood flow, optical coherence tomography, perfusion

Leber's hereditary optic neuropathy (LHON) is an inherited blinding disease characterized by degeneration of retinal ganglion cells (RGCs).[1,2] LHON is characterized by subacute loss of central vision due to the early involvement of smaller caliber fibers of the papillomacular bundle (PMB), as shown by postmortem and in vivo studies with optical coherence tomography (OCT).[3–6] Axonal loss is preceded by typical swelling of the optic nerve head (ONH), pseudoedema, leading to optic atrophy over a few months, with relative sparing of the far peripheral nasal quadrant. Peripapillary and ONH microangiopathy is a hallmark feature of presymptomatic and acute stages of disease, typically accompanying the pseudoedema, which resolves in the chronic stage. These vascular alterations hint at a possible role of the ocular vasculature in the still elusive pathogenesis of LHON. Various techniques, including fundus photographs,[7,8]

fluorescein angiography,[9] and, recently, optical coherence tomography angiography (OCT-A)[10–14] have been used to study the ocular vasculature in LHON, but none of these techniques can quantify optic nerve blood flow. Laser speckle contrast imaging (LSCI) allows to measure optic disk blood flow in a patient-friendly, noninvasive manner.[15–19] At present, LSCI measurements in LHON have been reported only in a case report.[20] The aim of this study was to characterize the optic disk blood flow in asymptomatic LHON mitochondrial DNA (mtDNA) mutation carriers and in the subacute disease stage of LHON, as compared to healthy controls using laser speckle flowgraphy (LSFG), a commercially available ophthalmic application of LSCI.

METHODS

Patients

The present study included 3 groups: (1) asymptomatic LHON mutation carriers, (2) LHON affected patients, and (3) control subjects. Eyes of patients with LHON were classified in four disease stages according to disease duration, as previously described: early subacute stage (disease duration <3 months), late subacute stage (3–6 months), dynamic stage (6–12 months), and chronic stage (>12 months).[12] LHON carriers and patients were examined at the IRCCS Istituto di Scienze Neurologiche di Bologna (ISNB), Bellaria Hospital, Bologna, at the University Vita-Salute, IRCCS Ospedale San Raffaele, Milan, and at the University Hospital of Parma. LHON diagnosis was molecularly confirmed at the Laboratory of Neurogenetics at ISNB, in Bologna. Controls were recruited from outpatients attending a routine ophthalmological examination and according to the following inclusion criteria: past and current normal ophthalmic findings, intraocular pressure (IOP) ≤21 mm Hg. Exclusion criteria for all participants were ametropia >3 diopters, significant opacities of the optical media (e.g. LOCS-III grading ≥2), tilted optic disk, diabetes mellitus, uncontrolled arterial hypertension as defined as systolic blood pressure >150 mm Hg and/or diastolic blood pressure >100 mm Hg, and neurodegenerative disease, such as Alzheimer's or Parkinson's disease. None of the patients or carriers had clinical and/or magnetic resonance imaging features of multiple sclerosis.

All participants underwent a comprehensive neurological and ophthalmological examination, which included autorefractometry, best-corrected visual acuity (BCVA) assessment with the standard Early Treatment of Diabetic Retinopathy Study chart, slit-lamp examination, IOP measurement, blood pressure measurement, OCT, LSFG and color fundus photography. The study was approved by the ethics committees of the involved centers and participants gave their informed consent after explanation of the nature and possible consequences of the study according to the Declaration of Helsinki. Parental informed consent was obtained for minors under 18 years of age.

Laser Speckle Flowgraphy

The principles of LSFG have been described in detail by Sugiyama.[15] The main output parameter, known as mean blur rate (MBR), is expressed in arbitrary units (AUs) and was shown to linearly correlate with absolute ONH capillary blood flow in animal studies.[21,22] In the present investigation, we used a commercially available LSFG RetFlow unit (Nidek Co., LTD, Aichi, Japan) consisting of a fundus camera supplied with an 830-nm diode laser and a digital charge-coupled device (CCD) camera. The device was equipped with an eye-tracker and with targets for internal and external fixation. LSFG measurements showed high reproducibility in clinical studies.[23,24] One LSFG scan consists of 118 images captured at a rate of 30 Hz for approximately 4 seconds. The most recent version of LSFG Analyzer software (version: 3.8.0.4; SoftCare, Fukuoka, Japan) was used for the analysis. This software version features enhanced removal of artifacts (due, for example, to gross vitreous floaters or eye-tracker errors). Two ONH scans were acquired by an experienced operator. All scans underwent an in-built quality check as provided by the vendor. All examinations were performed under nonmydriatic conditions in dim room illumination. An elliptical region of interest (ROI) was drawn in a semi-automated fashion to fit the ONH borders, having as a reference the color fundus photograph, as previously described.[25] Within each ROI, the mean perfusion in the ONH microvasculature (referred to as Mean Tissue [MT]) was calculated using the "Cross-section" automated segmentation tool of the software. The mean of two scans was then averaged. ROIs generated at baseline were reused in follow-up scans. An example of LSFG image and color fundus photograph is shown in Figure 1. The optic disk area was measured as number of pixels within the elliptical ROI. The LSFG disk area, as measured in pixels, showed moderate to strong correlation with the disk area, as measured on magnification-corrected pictures taken by fundus camera in healthy Japanese subjects.[26]

Optical Coherence Tomography

Optic nerve and macula OCT scans were obtained with the Cirrus HD-OCT (software version 7.0.2.5; Carl Zeiss Meditec, Inc., Dublin, CA, USA). Peripapillary RNFL thickness and thickness of combined ganglion cell layer + inner plexiform layer (GCIPL) between the outer border of the RNFL and the inner border of the inner nuclear layer were measured via the Optic Disc Cube 200 × 200 protocol and the Macular 512 × 128 protocol, respectively.[27]

Statistical Analysis

Categorical data are presented as absolute and relative frequencies, whereas numerical variables are presented as medians and interquartile ranges (IQRs). The joint effects of age, sex, spherical equivalent, disk area, group, and stage of disease on MT, RNFL thickness, and GCIPL thickness were examined by multivariable linear mixed-effects models with participants and eyes as nested random effects (taking into account interocular correlation and repeated measurements). The results are presented as restricted maximum-likelihood estimates of the linear effects, with profile-likelihood confidence intervals and P values by Satterthwaite's method. Spherical equivalent was included as a covariate to partially compensate for the retinal magnification due to individual differences in axial length. Theoretically, the MT should not be affected by retinal magnification because it is the average blood flow value within the optic disk borders, however, we applied the correction because it is unclear from previous studies whether MT is correlated with axial length.[28] All the analyses were performed in R free software environment. A P value < 0.05 was considered statistically significant.
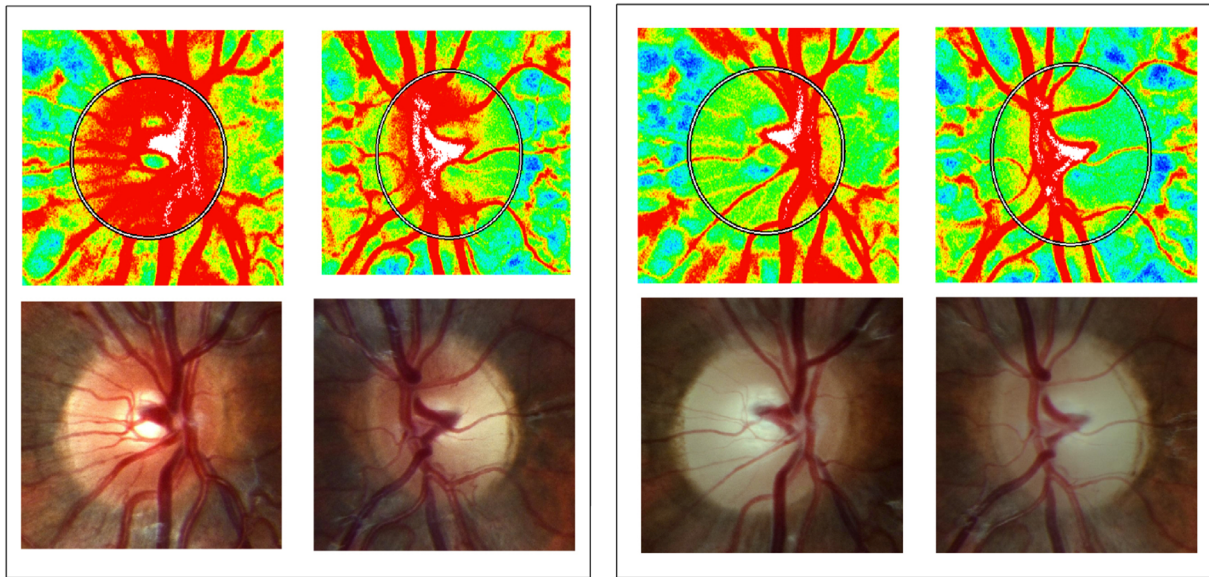
FIGURE 1. **Subacute LHON.** Pseudocolor LSFG maps and color fundus photographs of both eyes of one patient with LHON at baseline and follow-up visits (*left and right panels*, respectively). In the LSFG map, regions of higher blood flow are red and regions of lower blood flow are *blue*. The *ellipsoids* define the region of interest which was used to analyze optic nerve head (ONH) perfusion. At baseline, disease duration was 12 days and 3 months in the right eye and in the left eye, respectively. The follow-up visit was undertaken 5 months later. Note the different ONH pseudocolor at the follow-up visit, indicating a decrease in ONH perfusion as compared to the baseline visit.

RESULTS

Nineteen eyes of 10 LHON mutation carriers belonging to 6 families (5 men and 5 women), 15 eyes of 8 unrelated affected male patients with LHON and 40 eyes of 40 controls (21 men and 19 women) were included in the study. Molecular diagnosis of LHON carriers and patients are reported in Table 1. Supplementary Table S1 lists clinical, personal, and family history in detail for each patient. All patients with LHON had both eyes sequentially affected, except for one patient with the milder m.14484T>C mutation in the MT-ND6 gene, who had subclinical involvement in one eye, characterized by asymptomatic focal thinning of RNFL and

GCIPL, and, therefore, this eye was excluded from the study. Seven patients affected with LHON had at least 2 examinations: a baseline after a median interval of 4 months (range = 5 days to 11 months) from disease onset and a follow-up visit 3.5 months (range = 2–13 months) later, which was carried out at the same time of the day as the baseline visit to avoid the effects of circadian variations in optic disk blood flow.[29] Measurements of participants are summarized in Table 2 and represented graphically in the boxplots of Figure 2. RNFL thickness and GCIPL thickness significantly decreased with age ($P = 0.004$ for both), whereas the effect of age on MT was marginally nonsignificant ($P = 0.055$). Although not

TABLE 1. Demographics and Mutations of Included Carriers and Affected Patients

ID	Sex	Age at Baseline	Condition	Gene	Mutation
C1	M	13	Carrier	MT-ND4	m.11778G>A
C2	M	13	Carrier	MT-ND4	m.11778G>A
C3	M	18	Carrier	MT-ND4	m.11778G>A
C4	M	18	Carrier	MT-ND4	m.11778G>A
C5	M	21	Carrier	MT-ND1	m.3460G>A
C6	F	29	Carrier	MT-ND4	m.11778G>A
C7	F	48	Carrier	MT-ND4	m.11778G>A
C8	F	50	Carrier	MT-ND4	m.11778G>A
C9	F	53	Carrier	MT-ND4	m.11778G>A
C10	F	60	Carrier	MT-ND6	m.14484T>C
P1	M	15	Affected patient	MT-ND4	m.11778G>A
P2	M	15	Affected patient	MT-ND4L	m.10663T>C
P5	M	17	Affected patient	MT-ND4	m.11778G>A
P4	M	21	Affected patient	MT-ND1	m.3460G>A
P8	M	26	Affected patient	MT-ND6	m.14484T>C
P3	M	27	Affected patient	MT-ND4	m.11778G>A
P7	M	31	Affected patient	DNAJC30	c.152A>G p.Tyr51Cys (homozygous)
P6	M	34	Affected patient	MT-ND4	m.11778G>A

TABLE 2. Characteristics of Study Participants

	Controls	Carriers	LHON Early Sub-Acute	LHON Late Sub-Acute	LHON Dynamic	LHON Chronic
Subjects/eyes	40/40	10/19	5/6	7/11	4/7	4/5
Age, y	28.0 [24.0, 35.0]	25.0 [18.0, 49.5]	17.0 [15.0, 21.0]	26.0 [18.0, 29.0]	24.0 [16.5, 31.7]	21.5 [16.5, 28.0]
Sex = M (%)	21 (52.5)	5 (50.0)	5 (100)	5 (100)	5 (100)	5 (100)
MT (AU)	16.8 [15.0, 19.7]	15.1 [14.7, 19.2]	24.7 [24.2, 25.0]	14.3 [13.0, 16.6]	10.7 [10.3, 11.6]	10.8 [10.2, 11.3]
RNFL thickness, μm	93.0 [88.0, 99.0]	111.0 [95.6, 116.3]	109.0 [107.3, 119.5]	91.0 [77.7, 101.0]	84.0 [69.9, 94.0]	60.0 [54.0, 77.0]
GCIPL thickness, μm	85.0 [79.0, 88.0]	91.0 [86.5, 94.4]	66.0 [63.0, 72.0]	53.0 [50.7, 56]	54.0 [50.5, 57.0]	51.0 [46.0, 52.0]

Continuous data are shown as median and interquartile range. Age and sex refer to subjects, whereas MT, RNFL thickness, and GCIPL thickness refer to eyes.

Abbreviations: MT, mean tissue; AU, arbitrary unit; RNFL, retinal nerve fiber layer; GCIPL, ganglion cell + inner plexiform layer.
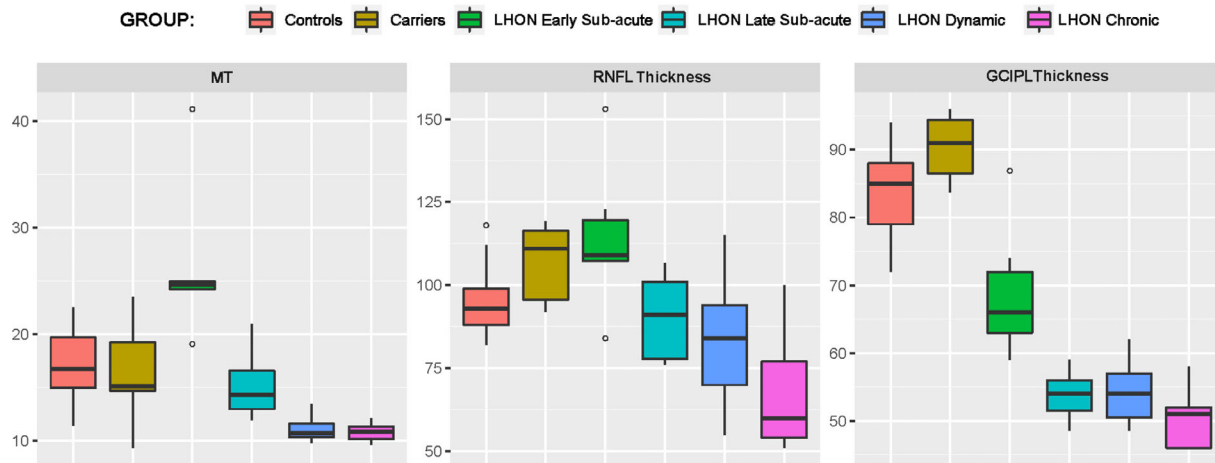

FIGURE 2. **Boxplots of all measurements of MT, RNFL thickness, and GCIPL thickness.** In each column, the *middle line* represents the median, the *ends* of the boxes represent 25th and 75th percentiles, and the *white circles* are the outliers. The scale is in arbitrary units for MT and in μm for RNFL thickness and GCIPL thickness. Abbreviations: MT, mean tissue; RNFL, retinal nerve fiber layer; GCIPL, ganglion cell + inner plexiform layer.

statistically significant, MT tended to decrease with increasing disk area ($P = 0.057$). Table 3 reports the comparisons between groups corrected for age, sex, spherical equivalent, disk area, and correlation between eyes of the same subject. Carriers had higher values of RNFL thickness, GCIPL thickness, and disk area than controls ($P = 0.018$, $P = 0.003$, and $P = 0.011$, respectively), whereas there was no difference in MT between the two groups ($P = 0.936$).

MT and RNFL thickness of LHON eyes in the early subacute stage were higher than in the controls ($P < 0.001$ and $P = 0.001$, respectively). MT declined below the values of controls during the late subacute stage ($P = 0.024$), whereas RNFL thickness became lower than in controls later during

the dynamic stage ($P < 0.001$). GCIPL thickness of affected patients was lower than in controls independently of the stage of the disease ($P < 0.001$). Disk area of patients affected with LHON was not significantly different from that of controls ($P = 0.186$).

Figure 3 graphically displays the temporal evolution of MT, RNFL thickness, and GCIPL thickness in LHON affected eyes, according to the standard score of controls values (i.e. the number of standard deviations above or below the controls mean). In agreement with the quantitative results presented above, the smoothed averages obtained by local polynomial regression showed that early subacute stage MT was more elevated above normal values and it

TABLE 3. Comparisons Between Groups

	MT	RNFL Thickness	GCIPL Thickness
Carriers versus controls	0.08 [−1.75 to 1.93] ($P = 0.936$)	8.21 [1.94, 14.49] ($P = 0.018$) *	5.34 [2.23, 8.45] ($P = 0.003$) *
LHON early acute versus controls	8.67 [5.92, 11.62] ($P < 0.001$) *	15.19 [6.99, 23.39] ($P = 0.001$) *	−17.01 [−21.12 to −12.93] ($P < 0.001$) *
LHON late acute versus controls	−2.73 [−4.90 to −0.55] ($P = 0.024$) *	−3.94 [−11.19 to 3.32] ($P = 0.315$)	−31.34 [−34.96 to −27.72] ($P < 0.001$) *
LHON dynamic versus controls	−5.96 [−8.65 to −3.33] ($P < 0.001$) *	−17.50 [−25.69 to −9.31] ($P < 0.001$) *	−32.80 [−36.89 to −28.71] ($P < 0.001$) *
LHON chronic versus controls	−6.51 [−9.57 to −3.55] ($P < 0.001$) *	−25.34 [−34.01 to −16.72] ($P < 0.001$) *	−35.09 [−39.42 to −30.79] ($P < 0.001$) *

Data are presented as estimates with 95% confidence intervals and *P* values.

Abbreviations: MT, mean tissue; RNFL, retinal nerve fiber layer; GCIPL, ganglion cell + inner plexiform layer.
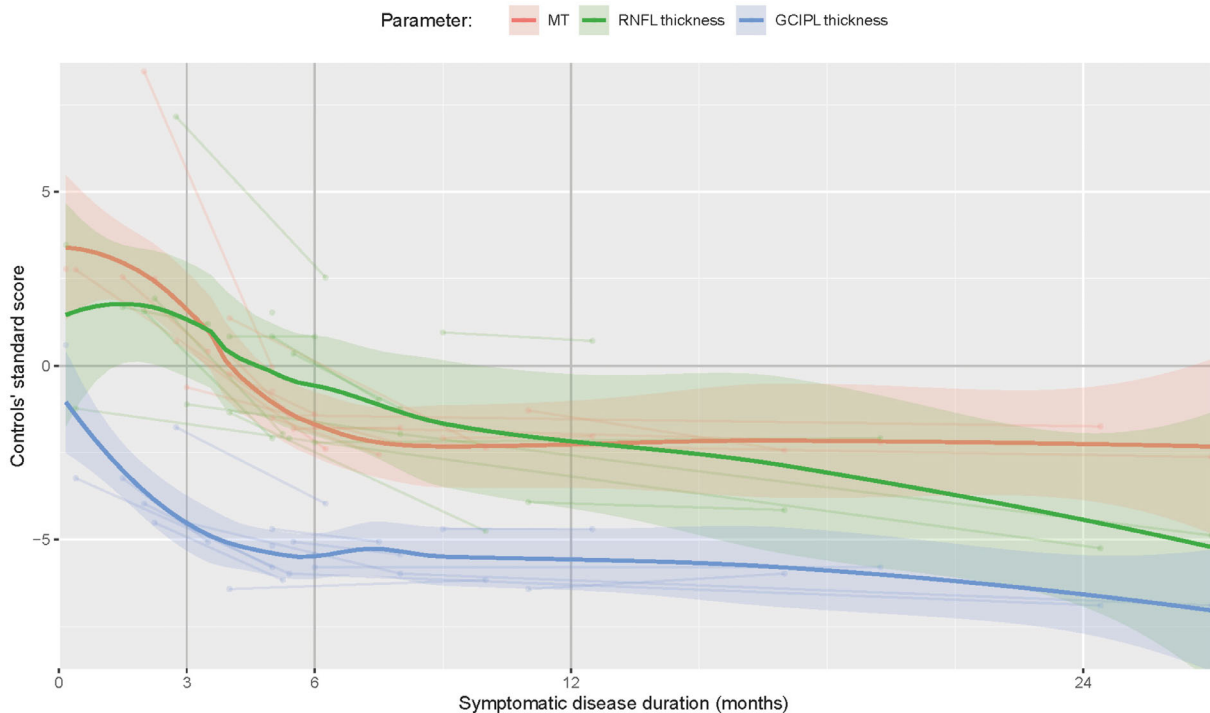
* = Statistically significant.

FIGURE 3. **Temporal evolution of MT, RNFL thickness, and GCIPL thickness according to symptomatic disease duration**. Each point represents a measurement, and the *straight lines* connect repeated measurements of the same eye. Smoothed averages and corresponding pointwise 95% confidence intervals were obtained by local polynomial regression. Abbreviations: MT, Mean tissue; RNFL, retinal nerve fiber layer; GCIPL, ganglion cell + inner plexiform layer. Controls' standard score = 0 corresponds to the mean value of controls.

subsequently declined more rapidly as compared to RNFL thickness.

DISCUSSION

The key finding of the present study is that the optic disks of patients with LHON within 3 months from clinical onset showed high blood flow as represented by the LSFG parameter MT. The high MT might be thus considered as a clinically useful marker of the disease in the diagnostic workup of LHON, especially in consideration of the relative paucity of pathognomonic features in LHON. We hypothesize that at least three nonmutually exclusive mechanisms lead to high MT. One possibility is that mitochondrial failure triggers a local response characterized by compensatory vasodilation and subsequent hyperperfusion. Nitric oxide release might be involved in vasodilation as a consequence of the possible pseudo-hypoxic state induced by the ongoing mitochondrial failure in RGCs and most importantly in their axons, which suffer the pseudoedematous swelling.[1,2] This latter has been variously interpreted, one hypothesis being axonal flow stasis with compensatory engulfment of proliferated mitochondria. Moreover, we cannot exclude the intermediation of glutamate toxicity, as previously documented in LHON cybrids.[30,31] Another possible mechanism could be the opening of microvascular shunts. In keeping with the so-called "compressive hypothesis," increased pressure within the ONH due to compartmental syndrome precipitated by the pseudoedema would shunt blood flow from the retinal to the choroidal circulation through the opening of the shunt microvessels, some of which lie on the optic disk area. Both mechanisms of dilation and shunting would fit with the previously reported peripapillary choroidal thick-

ening.[32] A third possibility is that the very localized events occurring in LHON, which are driven by functional peculiarities of RGCs as well as by anatomic constrains, may resemble stroke-like events (SLE) characterizing the mitochondrial encephalomyopathy, stroke-like episodes, lactic acidosis (MELAS) syndrome.[33] The links to LHON are supported by the fact that many rare LHON mutations may also lead to the MELAS phenotype, when the heteroplasmic mutational load is very high, but also by the histopathological evidence in LHON that small vessels at the ONH are affected by mitochondrial proliferation and dysfunction, very similarly to what is documented also in the cerebral vessels of patients with MELAS presenting SLE.[34] Thus, what is happening at the ONH in LHON might well be a very localized stroke-like event paralleling those seen in MELAS.

If, on the one hand, high blood flow seems to characterize the early subacute disease stage, on the other hand, we did not find a significantly different MT between asymptomatic carriers and controls. Of note, the carriers in our series are heterogeneous, including both young men and old women, thus representing a possible bias due to different age/gender predisposition to disease conversion. Although the present study does not support the presence of abnormal optic disk blood flow in the LHON carrier population taken as a whole, it cannot be excluded that modulation of optic disk blood flow may represent a compensatory mechanism to mitochondrial dysfunction in certain subgroups of carrier subjects. Moreover, measurement of blood flow under conditions of metabolic stress, such as during flicker light stimulation, could show a difference between LHON carriers and controls.[18] Further studies are needed to test if an increase in MT occurs in the preclinical stage immediately preceding the visual loss.

Moreover, optic disk blood flow might be influential on the risk of conversion, as previously hypothesized.[35] In this regard, an intriguing hypothesis is that blood flow impairment may be a mechanism through which tobacco smoking triggers conversion.[36] Chronic smoking is thought to lead to vascular dysfunction in the eye,[37] as well as to impair the compensatory activation of mitochondrial biogenesis.[36] Both mechanisms may synergistically lead to cross the threshold for energy shortage at the ONH and ease the conversion to affected in smokers.

We next analyzed the longitudinal structural and blood flow parameters in patients affected with LHON. The results demonstrated that GCIPL thickness is the first to be reduced below normal values. MT and RNFL thickness showed similar trends, with high values in the early subacute stage and a progressive decline thereafter. However, MT fell below mean normal values earlier than RNFL thickness. Axonal stasis, mitochondrial biogenesis, and a subsequent slow process of axonal clearance may contribute to delay RNFL thinning after GCIPL thinning and blood flow loss.[4,6]

We acknowledge some limitations in our study. First, the relatively small sample size. Second, there are limitations inherent in the LSFG technique, such as the lack of depth resolution. Changes in ONH structure may indeed affect laser penetrance and it is unclear to which degree the vasculature supplied by either the retinal or the posterior ciliary arteries contribute to the signal.[21] The current in-built analysis software has certain limitations as well. Indeed, although the MT calculation itself involves subtraction of the larger vessels, it sometimes happens that some of these vessels are not subtracted, especially when their blood flow is relatively low. In the future, an automated segmentation algorithm based on structural data (e.g. on vessel diameter) rather than on the MBR itself could further improve the discrimination between optic disk microvasculature and larger vessels in order to analyze these distinct (although not independent) optic disk vascular compartments separately. Third, the lack of correction of images for axial length differences is a limitation because the RNFL measurements are taken at different retinal locations in each subject, and the GCIPL thickness is integrated over a different retinal area in different subjects.[38] Because axial length measurements were not available, we applied a correction based on the spherical equivalent, but correction of the lateral scale before extraction of quantitative data is required to compensate for retinal magnification more accurately. The lack of OCT-A data is another limitation of this study. The combination of OCT-A and LSFG provides complementary information and the identification of the consistent of LSFG and OCT-A may provide more evidence for optic disk perfusion as a promising biomarker for LHON diagnosis and monitoring. OCTA allows for depth resolution down to the capillary level, but it cannot quantify perfusion. In contrast, LSFG provides a quantitative measure of perfusion, but it does not resolve individual capillary layers. Our results, together with previous OCT-A findings,[12] suggest that high peripapillary retinal vessel density is associated with high blood flow at the optic disk during the early subacute stage of LHON. Microangiopathy is a unique feature of LHON in contrast to ischemic or inflammatory optic neuropathies. The role of this feature in LHON is still unknown and we can hypothesize its potential compensatory role in carriers as well as its role as precipitating factor in the conversion to full-blown disease.

In summary, the present study compares for the first time the dynamics of optic disk blood flow, RNFL thickness, and GCIPL thickness during the early stage of LHON and in asymptomatic LHON carriers. Our data show an essentially normal perfusion of ONH tissue in asymptomatic LHON carriers, whereas in patients during the first 3 months of disease we observed high ONH perfusion declining to reduced perfusion during the following stages toward chronic disease. The dynamics of blood flow was similar to that of RNFL thickness, although MT showed a higher elevation above normal values, followed by a steeper decline. Further longitudinal studies integrating LSFG with OCT-A may help to further clarify the pathogenesis of LHON, characterizing the role played by microangiopathy and blood flow.

Overall, optic disk blood flow as measured with LSFG may become a promising biomarker for LHON diagnosis and monitoring, as well as an objective outcome measure for assessing response to therapies.

References

1. Carelli V, Ross-Cisneros FN, Sadun AA. Mitochondrial dysfunction as a cause of optic neuropathies. *Prog Retin Eye Res*. 2004;23(1):53–89.

2. Yu-Wai-Man P, Griffiths PG, Chinnery PF. Mitochondrial optic neuropathies - disease mechanisms and therapeutic strategies. *Prog Retin Eye Res*. 2011;30(2):81–114.

3. Pan BX, Ross-Cisneros FN, Carelli V, et al. Mathematically modeling the involvement of axons in Leber's hereditary optic neuropathy. *Invest Ophthalmol Vis Sci*. 2012;53(12):7608–7617.

4. Barboni P, Carbonelli M, Savini G, et al. Natural history of Leber's hereditary optic neuropathy: longitudinal analysis of the retinal nerve fiber layer by optical coherence tomography. *Ophthalmology*. 2010;117:623–627.

5. Balducci N, Savini G, Cascavilla ML, et al. Macular nerve fibre and ganglion cell layer changes in acute Leber's hereditary optic neuropathy. *Br J Ophthalmol*. 2016;100(9):1232–1237.

6. Hwang TJ, Karanjia R, Moraes-Filho MN, et al. Natural History of Conversion of Leber's Hereditary Optic Neuropathy: A Prospective Case Series. *Ophthalmology*. 2017;124(6):843–850.

7. Nikoskelainen E, Hoyt WF, Nummelin K. Ophthalmoscopic findings in Leber's hereditary optic neuropathy. I. Fundus findings in asymptomatic family members. *Arch Ophthalmol*. 1982;100:1597–1602.

8. Nikoskelainen E, Hoyt WF, Nummelin K. Ophthalmoscopic findings in Leber's hereditary optic neuropathy. II. The fundus findings in affected family members. *Arch Ophthalmol*. 1983;101:1059–1068.

9. Nikoskelainen E, Hoyt WF, Nummelin K, et al. Fundus findings in Leber's hereditary optic neuropathy. III. Fluorescein angiographic studies. *Arch Ophthalmol*. 1984;102:981–989.

10. Gaier ED, Gittinger JW, Cestari DM, et al. Peripapillary Capillary Dilation in Leber Hereditary Optic Neuropathy Revealed by Optical Coherence Tomographic Angiography. *JAMA Ophthalmol*. 2016;134(11):1332–1334.

11. Takayama K, Ito Y, Kaneko H, et al. Optical coherence tomography angiography in Leber hereditary optic neuropathy. *Acta Ophthalmol*. 2017;95(4):e344–e345.

12. Balducci N, Cascavilla ML, Ciardella A, et al. Peripapillary vessel density changes in Leber's hereditary optic neuropathy: a new biomarker. *Clin Exp Ophthalmol*. 2018;46(9):1055–1062.

13. Kousal B, Kolarova H, Meliska M, et al. Peripapillary microcirculation in Leber hereditary optic neuropathy. *Acta Ophthalmol*. 2019;97(1):e71–e76.

14. Yu J, Xu H, Huang Y, et al. Changes in Retinal Perfusion in Leber's Hereditary Optic Neuropathy: An Optical Coherence Tomography-Angiography Study. *Ophthalmic Res*. 2021;64(5):863–870.

15. Sugiyama T. Basic Technology and Clinical Applications of the Updated Model of Laser Speckle Flowgraphy to Ocular Diseases. *Photonics*. 2014;1(3):220–234.

16. Kunikata H, Nakazawa T. Recent Clinical Applications of Laser Speckle Flowgraphy in Eyes with Retinal Disease. *Asia Pac J Ophthalmol (Phila)*. 2016;5(2):151–158.

17. Witkowska KJ, Bata AM, Calzetti G, et al. Optic nerve head and retinal blood flow regulation during isometric exercise as assessed with laser speckle flowgraphy. *PLoS One* 2017;12:e0184772.

18. Mursch-Edlmayr AS, Pickl L, Calzetti G, et al. Comparison of Neurovascular Coupling between Normal Tension Glaucoma Patients and Healthy Individuals with Laser Speckle Flowgraphy. *Curr Eye Res*. 2020;45:1438–1442.

19. Calzetti G, Mora P, Romani A, et al. Optic nerve head and peripapillary perfusion as assessed with laser speckle flowgraphy in non-arteritic anterior ischaemic optic neuropathy. *Acta Ophthalmol*. 2021;99: e445–e446.

20. Watanabe T, Mashima Y, Kigasawa K, Mashima A, Shimura M, Hirakata A. Increased Microcirculation on Optic Nerve Head by Laser Speckle Flowgraphy at Early Stage of Leber Hereditary Optic Neuropathy. *Neuroophthalmology*. 2018;43(6):411–416.

21. Wang L, Cull GA, Piper C, et al. Anterior and posterior optic nerve head blood flow in nonhuman primate experimental glaucoma model measured by laser speckle imaging technique and microsphere method. *Invest Ophthalmol Vis Sci*. 2012;53(13):8303–8309.

22. Aizawa N, Nitta F, Kunikata H, et al. Laser speckle and hydrogen gas clearance measurements of optic nerve circulation in albino and pigmented rabbits with or without optic disc atrophy. *Invest Ophthalmol Vis Sci*. 2014;55(12):7991–7996.

23. Calzetti G, Fondi K, Bata AM, et al. Assessment of choroidal blood flow using laser speckle flowgraphy. *Br J Ophthalmol*. 2018;102(12):1679–1683.

24. Calzetti G, Mora P, Favilla S, et al. Assessment of choroidal neovascularization perfusion: a pilot study with laser speckle flowgraphy. *Trans Vis Sci Tech*.2020;9(5):9.

25. Calzetti G, Mursch-Edlmayr AS, Bata AM, et al. Measuring optic nerve head perfusion to monitor glaucoma: a study on structure-function relationships using laser speckle flowgraphy. *Acta Ophthalmol*. 2022;100:e181–e191.

26. Enomoto N, Anraku A, Tomita G, et al. Characterization of laser speckle flowgraphy pulse waveform parameters for the evaluation of the optic nerve head and retinal circulation. *Sci Rep*. 2021;11(1):6847.

27. Carta A, Mora P, Aldigeri R, et al. Optical coherence tomography is a useful tool in the differentiation between true edema and pseudoedema of the optic disc. *PLoS One*. 2018;13(11):e0208145.

28. Anraku A, Enomoto N, Tomita G, et al. Ocular and Systemic Factors Affecting Laser Speckle Flowgraphy Measurements in the Optic Nerve Head. *Transl Vis Sci Technol*. 2021;10(1):13.

29. Iwase T, Yamamoto K, Ra E, Murotani K, Matsui S, Terasaki H. Diurnal variations in blood flow at optic nerve head and choroid in healthy eyes: diurnal variations in blood flow. *Medicine (Baltimore)*. 2015;94(6):e519.

30. Beretta S, Mattavelli L, Sala G, et al. Leber hereditary optic neuropathy mtDNA mutations disrupt glutamate transport in cybrid cell lines. *Brain*. 2004;127(Pt 10):2183–2192.

31. Kaur C, Sivakumar V, Foulds WS. Early response of neurons and glial cells to hypoxia in the retina. *Invest Ophthalmol Vis Sci*. 2006;47(3):1126–1141.

32. Borrelli E, Triolo G, Cascavilla ML, et al. Changes in Choroidal Thickness follow the RNFL Changes in Leber's Hereditary Optic Neuropathy. *Sci Rep*. 2016;6:37332.

33. Carelli V, La Morgia C, Valentino ML, Barboni P, Ross-Cisneros FN, Sadun AA. Retinal ganglion cell neurodegeneration in mitochondrial inherited disorders. *Biochim Biophys Acta*. 2009;1787(5):518–528.

34. Yamadera M, Fujimura H, Shimizu Y, et al. Increased number of mitochondria in capillaries distributed in stroke-like lesions of two patients with MELAS. *Neuropathology*. 2019;39(5):404–410.

35. Ramos Cdo V, Bellusci C, Savini G, et al. Association of optic disc size with development and prognosis of Leber's hereditary optic neuropathy. *Invest Ophthalmol Vis Sci*. 2009;50(4):1666–1674.

36. Giordano L, Deceglie S, d'Adamo P, et al. Cigarette toxicity triggers Leber's hereditary optic neuropathy by affecting mtDNA copy number, oxidative phosphorylation and ROS detoxification pathways. *Cell Death Dis*. 2015;6:e2021.

37. Garhöfer G, Resch H, Sacu S, et al. Effect of regular smoking on flicker induced retinal vasodilatation in healthy subjects. *Microvasc Res*. 2011;82(3):351–355.

38. Llanas S, Linderman RE, Chen FK, Carroll J. Assessing the Use of Incorrectly Scaled Optical Coherence Tomography Angiography Images in Peer-Reviewed Studies: A Systematic Review. *JAMA Ophthalmol*. 2020;138(1):86–94.

Investigative Ophthalmology & Visual Science